CHAPTER 2

2. Literature Review

2.1 General

The Longwall method of coal extraction has been accepted worldwide as the most economical and safe method of underground mining. Its success in a given geo-mining condition critically depends on the rational design of its structures, such as the longwall face, chain pillars and gate roads. The functional objective of the chain pillar is to maintain the serviceability of gate entries, isolate the working panel from the goaf of the adjoining worked-out panel, and control the surface subsidence in some cases. The chapter presents the literature review of different aspects of chain pillar design in longwall mining. The study covers the stress redistribution due to longwall excavation and the mechanics of strata response, prevailing approaches to chain pillar design, the considerations of strength and loading of the chain pillar

2.2 Mechanics of Rock Damage and Stress Redistribution

In response to coal extraction from the sufficiently wide longwall face, the strata above the seam get disturbed in order of decreasing severity from the seam to the ground surface. As the face retreats to a sufficient distance from the starting line of the panel, the roof beds within the caving zone detach from each other in the middle, bend and sag. Curvilinear shape shear cracks are developed within a bed in a non-systematic manner to disintegrate it into a number of blocks of different sizes. These rock blocks fall freely onto the floor and are crowded randomly, increasing the volume of roof rocks. The size of the pile of rock fragments on the floor continues to grow as the face retreats further till it comes in contact with the fractured stratum. The sagging fractured stratum compresses the rock fragments in the goaf till the reactive pressure establishes mechanical equilibrium against the overburden load.

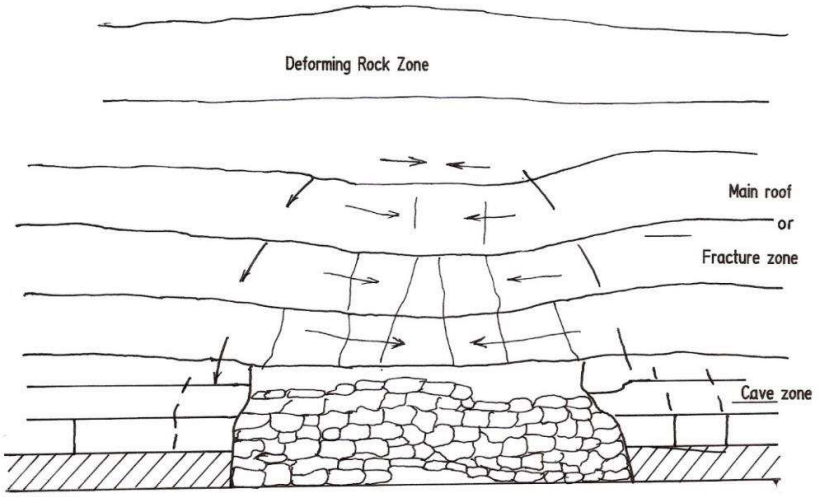

Figure 2.1 Damage zones above a longwall face

Based on the severity of the damage, three distinct zones of disturbance can be identified within the overlying strata (Singh and Kendorski, 1981). These are generally termed Caved, Fractured, and Continuous Deformation zones (Figure 2.1). The Caved zone includes rock fragments detached from their parent rock beds and have fallen freely onto the floor. The rock fragments undergo reconsolidation due to the sagging of strata in the Fractured zone and the heaving of the floor. The Fractured zone comprises rock blocks formed due to separation along the bedding planes and curvilinear fractures cutting through the beds (Das, 2000). The rocks in this zone lose cohesive resistance on the fracture planes (Shabanimashcool and Li, 2012). Hence, the constitutive behaviour of rock in this zone is significantly dependent on the strength properties of the rock joints.

On the other hand, the sparse presence of fractures in the Continuous Deformation zone hardly influences its mechanical behaviour. The strata within this zone are considered to deform elastically as a fixed-ended beam without developing major cracks along its length. The

subsidence at the ground can be observed due to the combined effect of the different extent of deformation in the three zones.

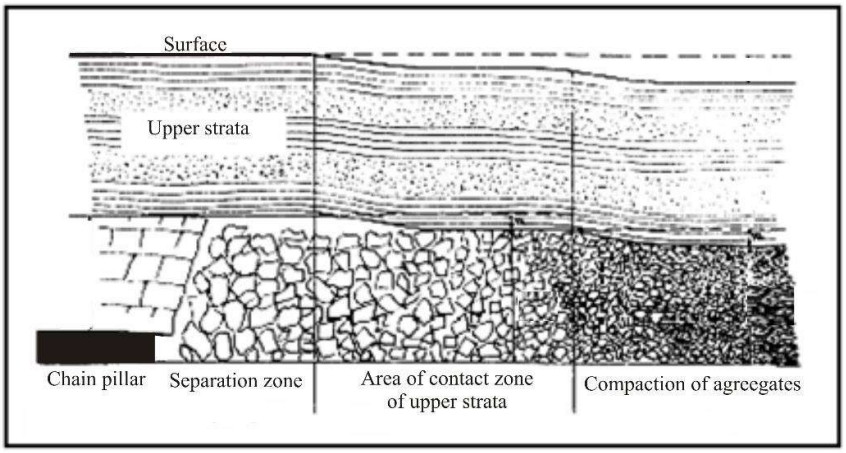

Figure 2.2 Probable strata condition in the vicinity of a longwall face with a weak immediate roof (modified after Sweby, 1997)

The rock fragments in the settled goaf are subjected to different degrees of compaction depending on their distance from the panel edge, the angle of repose of the rock fragments and the bending characteristics of the overlying fractured stratum (Figure 2.2). The goaf material at the panel edge is least compacted, whereas the goaf material around the centre is subjected to the maximum possible compaction. Based on the compaction state of the goaf material, the goaf area can be delimited into separation zone, zone of contact and zone of compacted aggregates in the order of increasing distance from the goaf edge (Sweby, 1997). In the separation zone, the goaf pressure is mainly due to the weight of the rock fragments in the goaf. The goaf pressure gradually in the zone of contact to achieve its maximum value at the centre of the zone of compaction.

Consequently, the recovered goaf pressure is the least at the panel edge. Still, it gradually increases to attain the maximum value at some distance into the goaf, known as the Cover

Pressure Distance (CPD). The width of these zones critically depends upon the strength and deformation characteristics of the overlying strata.

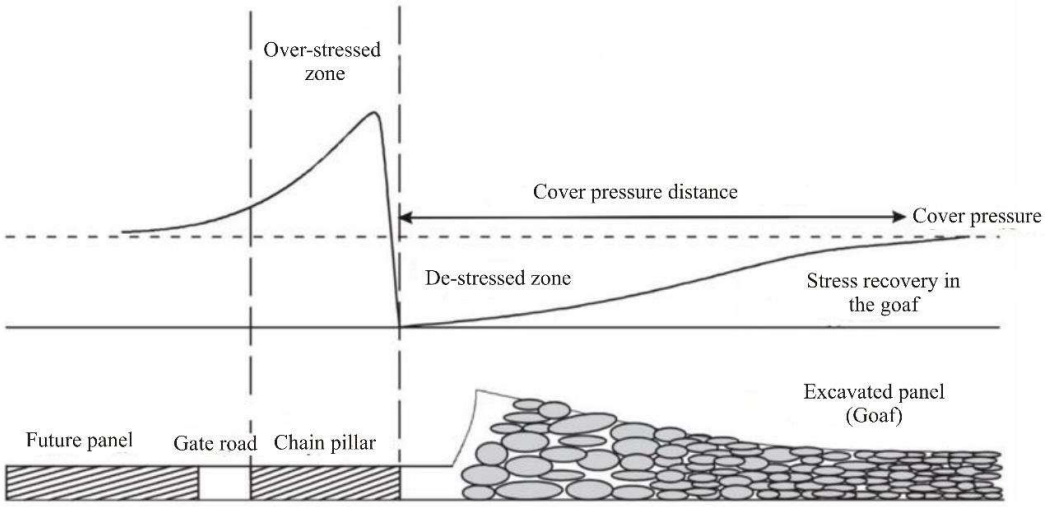

Figure 2.3 Redistribution of strata pressure at the seam level around the goaf area (modified after Yavuz, 2004)

Based on the observations of gate road stability behind the longwall faces, Wilson (1981) opined that the goaf pressure rises linearly from zero at the rib to the pre-mining cover pressure at 0.2 to 0.3 times working depth. Smart and Haley (1987) estimated CPD as 0.12 times the working depth for a specific case. King and Whittaker (1971) used the concept of shear angle, the angle between the vertical line at the edge of the panel and the caving line, to evaluate the loading on the pillar and the goaf. They implied that cover pressure is attained at a distance of Htanβ, where H and β are cover depth and shear angle, respectively. They suggested a shear angle of 31° for typical British conditions, which yields a CPD of 0.6 times the depth of working. Choi and McCain (1980) modified King and Whittaker's (1971) approach to the conditions prevailing in the US. They used the concept of negative angle of draw, equivalent to shear angle, to define the complete displacement zone on the goaf. They estimated a negative

angle of the draw of 18°, which evaluated the CPD as 0.32 times the working depth. Mark (1987) determined the shear angle as 21°from the field tests data, which estimated the CPD to be 0.38 times the depth of working for the US workings. Based on the observations in Indian mines, Sheorey (1993) opined that the CPD can be 0.2 and 0.3 times the working depth for stowed and caved goaf workings, respectively. The findings of these researchers show that the CPD ranges from 0.12 to 0.6 times the cover depth, depending on the geo-mining conditions (Figure 2.2).

The in-situ stresses are uniformly distributed in the coal seam. The state of the stress gets disturbed upon the development of the gate roads and extraction of the panels. The stresses are redistributed to achieve the new equilibrium condition. Consequently, a de-stressed zone develops in the roof of the excavated structure, and the redirected stresses are concentrated in the coal pillars. The zones where the induced vertical stress exceeds the pre-mining vertical stress are termed abutments, and the rock stress in these zones is called the abutment stress (Peng, 2006). The abutment stress ahead of the face and those along the sides of the panel are called the front and the side abutment stress, respectively. Since the maximum stress recovery in the ultimately settled goaf material can be less than or equal to the overburden load depending upon the width-to-depth ratio of the panel, the rear abutment is highly unlikely to exist. The abutment stresses intersect and superimpose on each other at the T-junctions (Figure 2.4), leading to an elevated abutment stress zone at the corner on both sides of the face. The maximum side abutment stress near the maingate and tailgate ribs begins to increase when the face is some distance in-bye and continues to reach the maximum value when the face has passed. However, the maximum front abutment stress is not uniformly distributed and can be located either at the corners or at the face centre, depending upon the geo-mechanical properties of the roof rocks, the width of the panel and the depth of cover. The weak immediate roof caves immediately behind the shield support and do not impose a strong weighting effect on the front

abutment (Peng, 2006). Therefore, the peak abutment stress is located at the panel corners and remains at this position as long as the weighting effects of the main roof do not come into action. Such conditions arise (a) when the immediate roof is thick and the main roof is located at a sufficient height above the coal seam so that the influence of its movement cannot be realised at the face; (b) during the non-weighting period. On the other hand, when either the immediate roof is thin, and the main roof is located close to the seam or is strong, a heavy weighting is realised at the face leading to a shift of the peak abutment stress at the face centre during the weighting period.

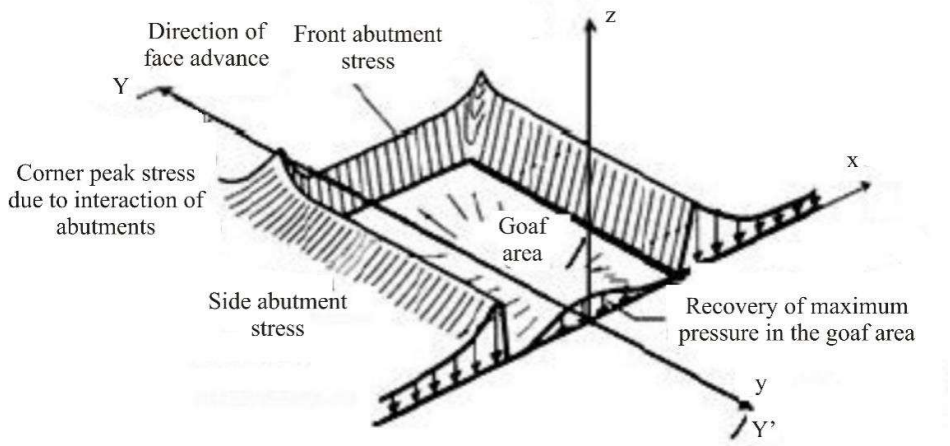

Figure 2.4 Distribution of the vertical stress in the coal seam

If the caving span is larger than the face length, which may be the case in shallow depth working with a shorter face length and the strong overlying strata, the weighting effects can be realised on the side abutments. According to Kirchhoff's elastic plate theory, the development of fracture in the main roof and the associated process of weighting is a function of lateral dimensions ('a' and 'b') of the plate structure of the main roof (Figure 2.5) (Qian and He, 1989). The first crack always develops at the middle of the longer axis of the plate top and then

extends along the longer side, followed by the shorter side in the goaf area. The interconnection of these cracks leads to the collapse of the main roof plate structure as it reaches its limiting value. If the (a/b) <1, the weighting effect of the main roof is felt at the front abutment (Case I). Otherwise, the weighting effect is realised at the side abutment (Case II).

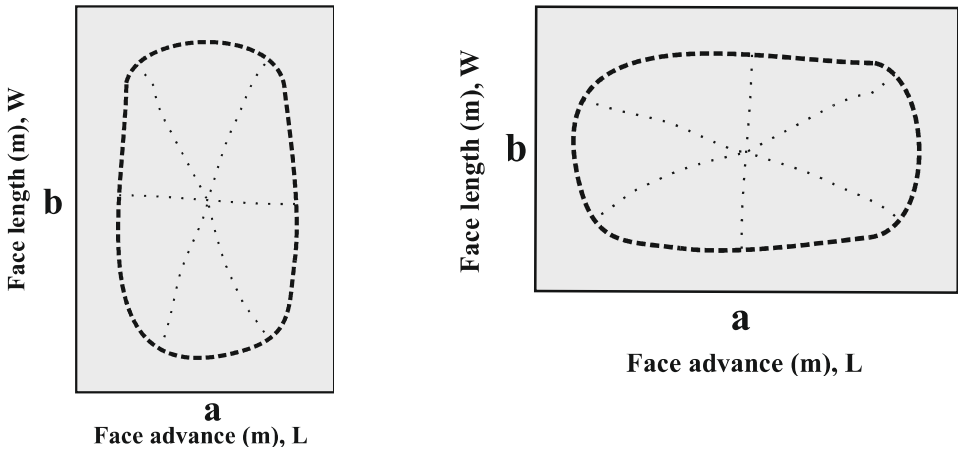

Case1: a/b<1 Case 2: a/b>1

Figure 2.5 Main roof failure for different ratios of the lateral dimensions (Qian and He, 1989)

The peak abutment stress significantly depends on the site-specific panel width, cover depth, extraction height, and the physicomechanical properties of the coal seam and roof rocks in a given mining condition (Jeremic, 1985; Majumder and Chakrabarty, 1991). Peng and Chiang (1984) and Whittaker and Singh (1979) observed that the peak abutment stress varies between 1.5 – 5 and 4 – 5 times the in-situ vertical stress in the US and UK conditions, respectively. Singh and Singh (2010) noted that the peak abutment stress ranges between 2 – 5 times the in-situ stress in the Indian geo-mining conditions. Rezaei et al. (2015a) noted the maximum abutment stress of 1.75 - 1.85 times the in-situ stress in Iranian conditions, while Guo et al. (2013) reported 1.5 - 2.5 times the in-situ stress in China.

The abutment stresses decrease from the edge of the panel to return to overburden load at some distance into the solid coal, called the Load Transfer Distance (LTD). Based on the measurements at five US longwall mines, Mark (1987) found a quadratic relation for the decay of stress with the distance from the edge of the panel. Wilson (1983) proposed an exponential decay profile of the abutment stress based on observations in British conditions. Based on the subsidence calibrated numerical modelling study, Yadav et al. (2020a, 2020b) reported that Wilson's (1983) exponential decay profile can characterise the non-uniform distribution of abutment stress in Indian conditions. Singh et al. (2011) also found a similar decay relationship based on the field measurements at sixteen Bord and Pillar workings in India.

The LTD is significantly dependent on the cover depth and the geo-mechanical properties of the overlying strata (Peng and Chiang, 1984; Larson et al., 2012; Larson et al., 2015; Singh et al., 2011; Yadav et al., 2020a; Yadav et al., 2020b). Based on the field measurements in the US conditions, Peng and Chiang (1984) found that the LTD increases with the cover depth such that $LTD\ (m) is\ 5.13\sqrt{H\ (m)}$. Larson et al. (2012) noted that the LTD greatly depended on the geo-mechanical properties of the overburden strata at a deep longwall mine in the Western US with strong and massive overburden strata. The LTD was two to four times greater than the estimate arrived from the empirical relationship of Peng and Chiang (1984). Larson et al. (2015) found a negative exponential relationship of LTD with depth based on field measurements of LTD at various Western US mines. They observed a significantly larger LTD than the value predicted by Peng and Chiang (1984). Similar observations were made by Yadav et al. (2020a, 2020b) for supercritical and subcritical longwall workings in India. They found a much larger LTD (1.8 – 2.7 times) compared to that predicted by Peng and Chiang (1984). Singh et al. (2011) proposed a linear relation of LTD with cover depth and Cavability Index for shallow depth Bord and Pillar workings in India.

When the geo-mining conditions are conducive, the deformation resulting from the longwall extraction and the damage to the superjacent strata extends up to the surface, forming a subsidence trough. Sheorey et al. (2000) noted that discontinuous or continuous subsidence could be observed for shallow to moderate depth workings in Indian geo-mining conditions. They found that the non-effective with-to-depth (NEW) ratio – the maximum width of extraction for a given cover depth for which no subsidence is expected at the surface, varies approximately from 0.2 to 0.8 in Indian conditions depending on the competence of the strata. They further reported that the angle of draw differs considerably from 9-25° in Indian coalfields depending upon the strata conditions. Singh and Yadav (1995) observed three different types of subsidence in Indian coalfields under different geo-mining conditions (Figure 2.6). Continuous subsidence is observed in deep mines, whereas stepped subsidence is observed in coal mines with shallow cover depth and strong (rigid) overburden. A continuous subsidence profile with many small steps is observed in coal mines with weak overburden strata.

Saxena (2003) developed an empirical model to estimate maximum subsidence in different Indian geo-mining conditions. This empirical model was derived from the field measurements of subsidence at several longwall panels under shallow to moderate depth of cover for predicting the subsidence under varying Indian geo-mining conditions. He found that the maximum surface subsidence is the function of the nature of strata, cover depth, extraction height, percentage of extraction, and goaf treatment (caving or stowing). In contrast, the angle of draw primarily depends on the nature of the strata. The maximum subsidence was observed at the centre of the profile, while the subsidence at the panel edge and half of the distance from the centre of the subsidence trough to the edge were one-fifth and one-half of the maximum subsidence, respectively.

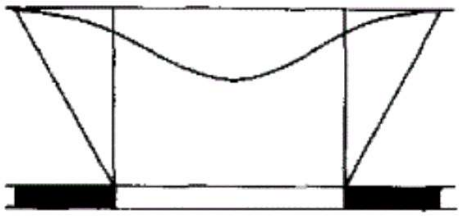

(a) Continuous subsidence profile

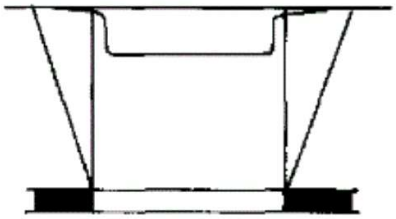

(b) Stepped subsidence profile

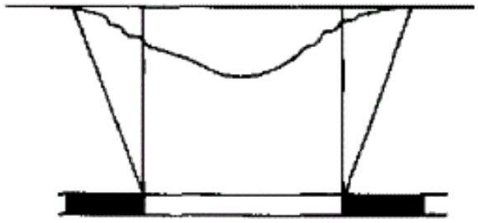

(c) Continuous subsidence profile with many steps

Figure 2.6 Subsidence observed in Indian coal mines (after Singh and Yadav, 1995)

The extent of damage in the overlying strata due to the longwall mining depends on extraction height, panel dimensions, cover depth, in-situ stresses, goaf treatment (caving or stowing), properties of the overlying strata, location of the strong strata, and corresponding expansion coefficient (Majdi et al., 2012; Singh and Singh, 2009; Peng 2006). The damaged strata in the overlying strata are categorised into three distinct disturbed zones: Caved zone, Fractured zone, and Continuous Deformation zone. Singh and Kendorski (1981) noted that caving height depends on the extraction height and the strength and stratigraphy of overlying roof strata, generally ranging from 3 – 6 times the extraction height. Karmis et al. (1983) opined that the

thickness of the caving zone could be 12 times the thickness of the mined coalbed. Based on the inter-burden deformation measurements above six longwall panels, Styler (1984) reported that the caving height of 8 to 12 times the extraction height, whereas the Fractured zone extended up to 50 times the extraction height above the coal seam. According to Palchik (1989), the thickness of the Fractured zone varies from 20 to 100 times the extraction height, and the Continuous Deformation zone lies above the Fractured zone, where no major fractures are present. Based on extensive field measurements, Zhou (1991) found that the height of the Caved and the Fractured zones vary as a function of extraction height. Peng (1992) opined that the combined height of the caved and Fractured zones varies from 20 to 30 times the mining height and is greater for hard strata and vice-versa.

Chekan and Listak (1993) noted that the height of the Caved zone is 2 – 20 times the extraction height, whereas the thickness of the Fractured zone ranges from 20 – 50 times the mining height. The Continuous Deformation zone is situated between the Fractured zone and the ground surface. According to the field measurements reported by Zhang et al. (2011), the thickness of the Caved zone and the Fractured zone is about 5-6 times and 10-11 times the mining height. Peng (2006) reported that the height of the Caved zone might vary from 2 to 8 times the extraction height depending on the geological conditions, while Karacan (2010) opined that the caving height ranges from 4 to 11 times the extraction height. Singh and Singh (2011) reported that the caving height could be as high as 15 times the extraction height in Indian geo-mining conditions where the presence of massive sandstone rocks dominates the overlying strata. Peng and Chiang (1984) estimated the thickness of the Fractured zone as 28 to 42 times the extraction height.

2.3 Progressive Loading of Chain Pillars

The loading of chain pillars is a complex and progressive phenomenon. It depends on numerous factors such as cover depth, overburden density, stiffness of the superincumbent strata,

abutment angle, spanning characteristics of the roof rocks overlying the disturbed zones, stiffness of goaf material, and the position of the longwall face relative to the chain pillar location (Mark 1987). A chain pillar is subjected to progressive loading commensurating with the stages of extraction in the adjoining longwalls. There are five stages of chain pillar loading, as depicted in Figure 2.7.

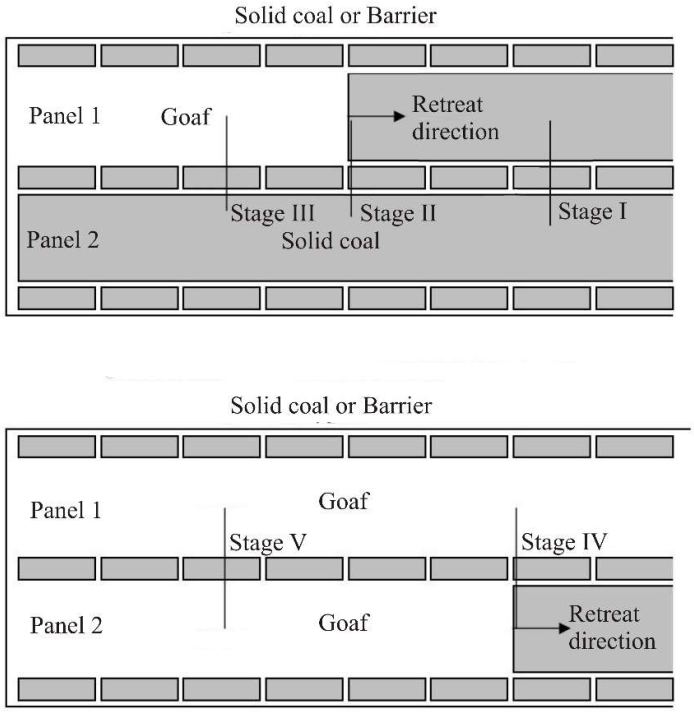

Figure 2.7 Schematic diagram depicting various stages of loading of a chain pillar

The pillar load in Stage I is mainly due to the development of the gate road and the cross-cuts within the zone of influence of the pillar. As the face of the first longwall panel approaches the pillar, the onset of front abutment pressure contributes to the loading Stage II, in addition to the load developed in Stage I. Stage III considers loading of the pillar due to one-sided goaf when the pillar is out of the influence of the face position. When the second longwall panel

retreats, the pillar is again subjected to front abutment loading in addition to the previous loads. This constitutes stage IV of the loading. In stage V, the second face retreats past sufficiently away from the pillar, and pillar loading is due to the double-sided goaf. The pillar is subjected to the maximum load at this stage.

The load on the pillars at the first stage is due to the weight of superincumbent strata immediately above the pillar and the tributary area. Tributary Area theory is widely employed for the estimation of development load (Wilson, 1972a; King and Whittaker, 1971; Mark, 1987; Carr and Wilson, 1982; Choi and McCain, 1980). However, the theory is based on certain underlying assumptions, such as a substantial ratio of the extraction span to the working depth and a negligible influence of the boundary effect of the panel edge on the pillar load (Sheorey and Singh, 1974). According to the theory, the development load per unit length of the roadway is given as follows (Mark, 1987):

$$L_D = Hw\gamma \tag{2.1}$$

where, H, w, and γ are depth of cover, pillar width and the average unit weight of overlying strata, respectively.

Mark (1987) pointed out that the Tributary Area theory makes a conservative (upper bound) estimate of the pillar load. Other crucial factors, such as the relative stiffness of the roof, pillars and floor, high horizontal stresses, width of the gate entry system, and decreased pillar stiffness caused by high extraction ratio, may affect the pillar load. Hence, numerical modelling is a reliable tool for determining the pillar load.

Stages II and IV of the chain pillar loading involve front abutment load due to the first and the second longwall face, respectively. Estimating the front abutment load on the pillar is difficult as it involves the non-uniform and unequal load distribution amongst the solid coal ahead of the face, goaf material, and chain pillars, depending upon their effective stiffness relative to each other. The estimation of front abutment load is genuinely a three-dimensional problem.

However, such a modelling procedure requires considerable time for the final solution. Further, selecting a proper constitutive model to represent the mechanical behaviour of the solid coal and goaf material can be difficult under an increased level of load (Sinha and Walton, 2019a). In such circumstances, the field measurements backed by empirical relations can be used to determine these loads. Mark (1987) empirically characterised the front abutment load based on the field measurements in the US longwall mines. He found that the front abutment load (L_f) was considerably lower compared to the side abutment load (L_s) and can be estimated using the relation $L_f = F(L_s)$, where 'F' is the front abutment factor. He suggested F = 0.5 for front abutment load due to the first longwall face and 0.7 for the second longwall face in US conditions. Based on the analysis of field measurements, Colwell (1998) also found F = 0.5 to be suitable for front abutment load due to the second longwall face in general Australian conditions.

The side abutment load of the first longwall face mainly contributes to the loading of the chain pillars in Stage III, whereas the side abutment loads of the first and second longwall faces lead to the loading of the pillar in Stage V. The side abutment load is generally determined using the concept of the abutment angle (β). The term 'abutment angle' has also been referred by 'negative angle of draw' and 'shear angle' (Choi and McCain 1980, King and Whittaker 1971). In these works, the abutment angle considers the mathematical approximation of the physical reality to estimate the transferred overburden load from above the goaf onto the pillar rather than the actual measurable goaf characteristics (Mark, 1990; Cowell, 1998; Sinha and Walton, 2019a).

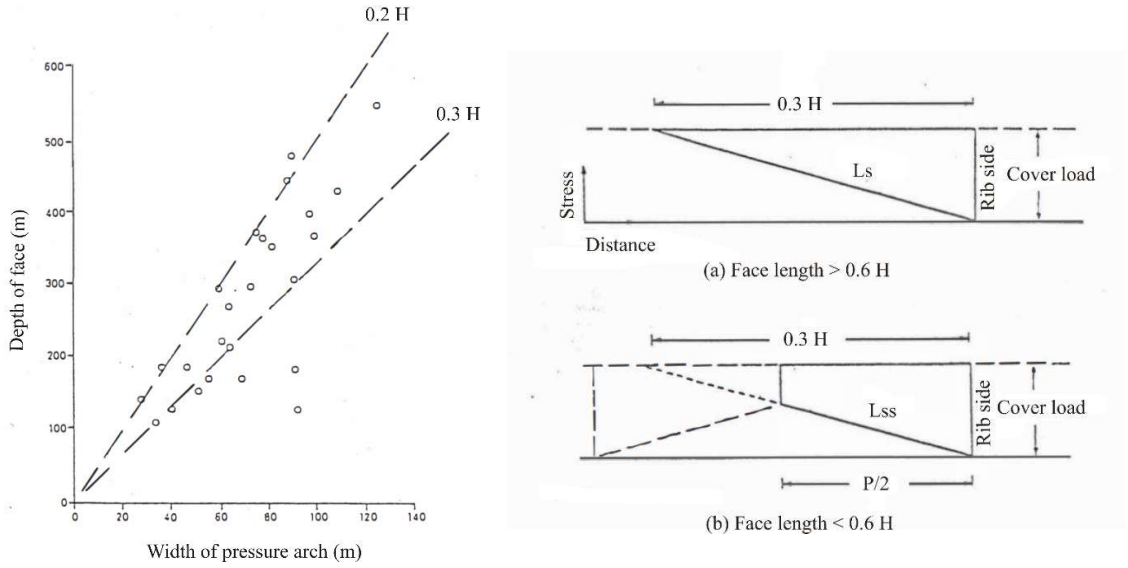

(i) (ii)

Figure 2.8 (i) Maximum width of pressure arches observed in British mines and (ii) schematic diagram of load deficiency in the goaf (Wilson, 1972b)

Wilson (1972b) utilised the 'stress balance' concept to evaluate the side abutment load in Great Britain mines (Figure 2.8). According to this concept, the 'stress deficiency' in the goaf area must be taken up by the unmined coal around it as the total vertical load due to the weight of overburden must be constant. Based on the observations of convergence in the gate road next to the extracted panel and the pressure arch theory, he suggested that the goaf pressure increases linearly from zero at the edge behind the face to the pre-mining cover pressure at the distance of 0.3 times the cover depth (Figure 2.8b). For a subcritical panel with a width less than 0.6 times the cover depth, the goaf pressure rises linearly from the edge but never attains the cover pressure. Hence, the panels having different width to depth ratio necessitates different expressions for evaluating side abutment load (Eq. 2.2-2.3).

$$L_s = 0.15\gamma H^2 \tag{2.2}$$

$$L_{ss} = \frac{1}{2} P\gamma \left(H - \frac{P}{1.2} \right) \tag{2.3}$$

where, L_s = side abutment load per unit length of gate entry for critical and supercritical panels,

L_{ss}= side abutment load per unit length of gate entry for subcritical panels,

P = width of the panel, and

γ = unit weight of the overburden rocks

Wilson (1972b) opined that the pressure rise in the goaf also depends on the development of the subsidence trough. The presence of strong strata near the seam could result in a heavy periodic weighting, which imposes a more significant abutment load on the pillars. King and Whittaker (1971) considered that the redistributed stresses at the seam level after extraction should be related to the subsidence profile at the surface. They introduced the concept of a 'shear angle (β)' over the goaf to define the loading of the pillar and suggested that the angle should be equal to the angle of draw, which is 31° for typical British conditions. Figure 2.9 depicts the 'line of shear' and the angle of shear subtended by shear and the vertical lines at the panel edge. If the panel width is less than $2Htan\beta$, shear lines intersect below the surface; otherwise, they extend up to the surface. Side abutment load for subcritical panels can be estimated using Equation 2.4, while Equation 2.5 can be used for critical and supercritical panels.

$$L_{ss} = \left(\frac{HP}{2} - \frac{P^2}{8tan\beta} \right) \gamma \tag{2.4}$$

$$L_s = H^2 (tan\beta) \frac{\gamma}{2} \tag{2.5}$$

where, 'H' and 'P' are panel width and length, respectively, and γ is the unit weight of the rocks.

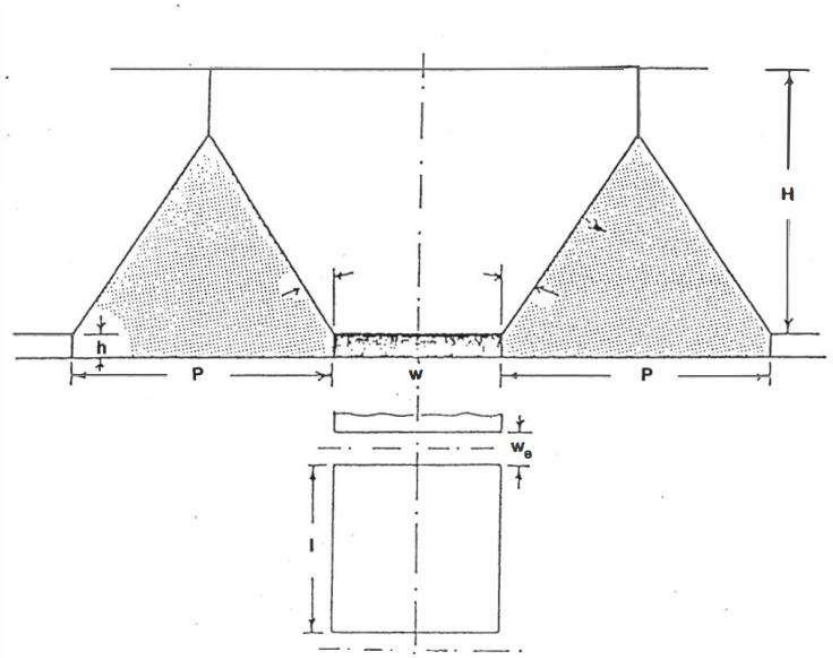

Figure 2.9 The estimation of the load on the chain pillar using the concept of shear angle (after Whittaker, 1983)

Choi and McCain (1980) modified the approach of King by introducing the concept of 'Complete Displacement Zone', defined as the entirely settled zone above the mined-out panel, which is not further affected by the extraction of the adjacent panel (Figure 2.10). The side abutment load is due to the rocks outside this zone. They defined the complete displacement zone using 'negative angle of draw', which is equivalent to the angle of shear in King and Whittaker (1971). Using subsidence data, Choi and McCain estimated the negative angle of draw to be 18° for the Pittsburgh seam.

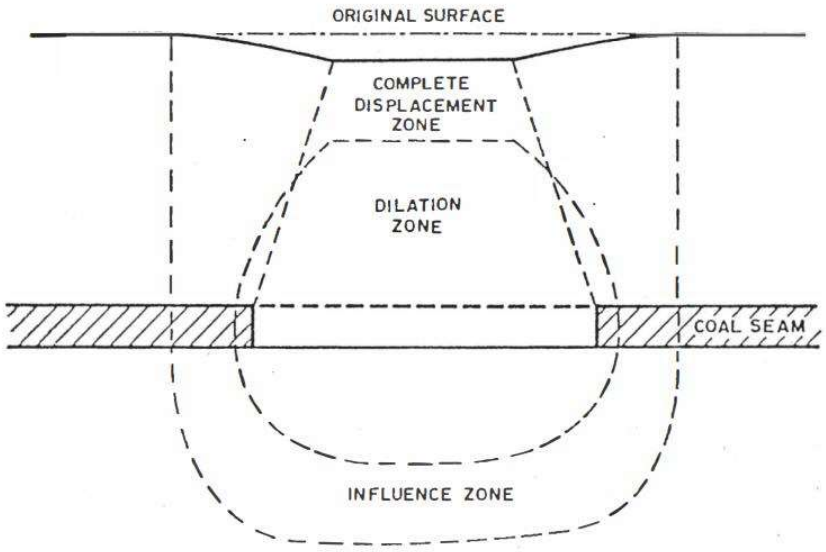

Figure 2.10 Overburden displacement zone above a mined-out longwall panel (after Choi and McCain, 1980)

Sheorey (1993) noted that the Wilson approach overestimates the abutment load for one-sided goaf. He developed an alternative method to determine the side abutment load for such conditions using the theory of beams on elastic foundations to define the exponential decay of abutment stress along with stabilisation of the goaf pressure at a distance of 0.3 and 0.2 times the cover depth for caved and stowed goaf, respectively. Equations 2.6 and 2.7 estimate the abutment load for subcritical and critical/supercritical panels.

$$L_{ss} = \frac{\gamma H(l+B)}{wl}\left\{w + \frac{B}{2} + 0.147H(0.4 + e^{-z}\sin z - 0.4e^{-z}\cos z) - \left[0.15H - \frac{P}{2H}\left(H - \frac{P}{1.2}\right)\right][1 - e^{-z}]\right\} \quad (2.6)$$

$$L_s = \frac{\gamma H(l+B)}{wl}\left[w + \frac{B}{2} + 0.147H(0.4 + e^{-z}\sin z - 0.4e^{-z}\cos z)\right] \quad (2.7)$$

where, L_{ss} is the side abutment load for the subcritical panel (width, P <0.6H), L_s is the side abutment load for critical and supercritical panels (P > 0.6H), H is the cover depth. B, w, and l are the bord width, pillar width, and pillar length, respectively, and γ is the unit weight of the overlying rocks. The parameter 'z' can be determined using the expression:

$$z = \frac{\pi}{0.12H}\left(w + \frac{B}{2}\right) \tag{2.8}$$

Frith and Reed (2019) observed that the load on the pillars is influenced by the bridging capability of the overburden strata. The pillar load is influenced by the caving height of strata as well (Rezaei et al., 2015b). With increased caving height, the pillar is subjected to increased load as the goaf stress recovery decreases due to the poor bulking factor of roof rocks (Yavuz, 2004). The load on the pillar is directly proportional to the unit weight of the overburden strata (Cowell, 1998).

Mark (1990) found a wide range of abutment angles varying from 10.7 to 25.2° for the longwall panels at the cover depth of 139 – 232 m based on the in-situ measurements in US coal mines (Table 2.1). He suggested an abutment angle of 21° as a conservative estimate of the abutment load in these conditions. Colwell (1998) opined that the abutment angle of 21° was appropriate for most Australian coal mining conditions. Colwell (1998) suggested an abutment angle of 26° for Central Colliery and 10° for Southern Coalfield mines. Das (2000) reported a wide variation in abutment angle, from less than 5° to greater than 65°, depending on the geo-mechanical properties of the strata in Indian coal mines.

Table 2.1 Abutment angle observed by various researchers

Refs.	Abutment angle (β°)	Depth (H, m)	Remarks
Mark (1992)	10.7°-25.2°	$139 \leq H \leq 232$	Back-calculated from the abutment load measurements from five US mines
Das (2000)	<5° to >60°	$H < 500$	Based on the field observations in Indian coal mining conditions
Tulu and Heasley (2012)	$\beta = 21°$ $\beta = 21° \left(\frac{H}{274.32}\right)^{-1.59}$ (2.9)	$H < 274$ $274 \leq H \leq 625$	Back-calculated based on field measurements in the US and Australian conditions employing analytical and numerical methods
Hill et al. (2015)	$\beta = 21.62 - 0.0221H + 0.0725w - 6.23C$ (2.10) where, w is the pillar width (m), C is the panel span criticality (=1 for W/H <0.75, =0 for W/H ≥0.75), W is the panel width	$H < 625$	Used for estimation of maingate loading conditions Based on the back-analysis of Australian and the US measurements data
Tuncay et al. (2021)	$\beta = 21°$ $\beta = 29.42 \times 0.68^{\left(\frac{H}{P}\right)}$ (2.11) Where P is the panel width (m)	$H < 200$ $200 \leq H \leq 625$	$\left(\frac{H}{P}\right)$ varies from 0.7 to 3.5

Tulu and Heasley (2012) analysed the combined database of field measurements for abutment loads in Australian and US conditions to back-calculate the abutment angle. They found that the abutment angle is not constant but varies with the mining depth. They suggested an abutment angle of 21° for depth less than 274 m with a negative correlation for greater depth. Hill et al. (2015) found a linear relation of the abutment angle with the cover depth, pillar width, and the face advance for the US and Australian conditions. Tuncay et al. (2021) observed that the abutment angle varies as the function of the panel depth to width ratio for depth greater than 200 m.

2.4 Strength of the Pillar

Several relations (Table 2.2) have been proposed based on Rock Mechanics theories, laboratory and in-situ testing, and back-analysis of failed and successful cases for estimating the strength of pillars.

Table 2.2 Pillar strength formulae developed by different authors

Reference	Equation	Derivation method	Shape of the pillar	Remarks
Holland and Gaddy (1957)	$S = 0.16k\frac{\sqrt{w}}{h}$ (2.12)	Lab tests	Slender	k_c is the strength of 25 mm cubic coal sample
Bieniawski (1968)	$S = k\left(0.64 + 0.36\frac{w}{h}\right)$ (2.13)	In-situ tests	Slender	k_{cr} is the strength of 30 cm cubical coal sample (critical size)
Mark and Chase (1997)	$S = 6.2\left(0.64 + 0.54\frac{w}{h} - 0.18\frac{w^2}{hl}\right)$ (2.14)	In-situ tests	Squat	Constant strength for in-situ coal
Salamon and Munro (1967)	$S = 7.2\frac{w^{0.46}}{h^{0.66}}$ (2.15)	Pillar case studies	Slender	Constant strength for in-situ coal
Salamonand Wagner (1985)	$S = 0.79k\frac{R_p^{0.59}}{V^{0.667}}\left\{\frac{0.59}{\varepsilon}\left[\left(\frac{R_p}{R_0}\right)^{\varepsilon} - 1\right] + 1\right\}$ (2.16) Where R_0 is critical $\frac{w}{h} = 5$, $R_p = \frac{w}{h}$ of the pillar, V=pillar volume, ε_p is a constant (=2.5)	Pillar case studies and Laboratory tests	Squat	For $\frac{w}{h} > 5$ k_{cr} is the strength of 30 cm cubical coal sample (critical size)
Sheorey et al. (1987)	$S = 0.27k_c h^{-0.36} + \left(\frac{H}{250} + 1\right)\left(\frac{w}{h} - 1\right)$ (2.17)	Theoretical, empirical methods and case studies	Slender and squat both	Considers In-situ stresses as well k_c is the strength of 25 mm cubic coal sample
Wilson (1972a)	(All equations are in ton and ft units) Case I $w > 2\bar{x}$ <u>Rectangular pillars</u> $S = \frac{4\gamma H}{wl}[wl - 1.5(w + l)hH \times 10^{-3} + 3h^2H^2 \times 10^{-6}]$ (2.18) <u>Long pillars</u> $S = \frac{4\gamma H}{w}(w - 1.5hH \times 10^{-3})$ (2.19)	Theoretical analysis	Slender and squat both	

	Case II $w \leq 2\bar{x}$ Rectangular pillars $S = 667\gamma \frac{w}{lH}\left(w_1 - \frac{w}{3}\right)$ (2.20) Long pillars $S = 667\gamma \frac{w}{H}$ (2.21) $\bar{x} = 0.0015hH$ (2.22) is the failed zone $\gamma = o.0707tft^{-3}$ is the rock density			
Galvin et al. (1999)	$S = 5.12\left(0.56 + 0.44\frac{w}{h}\right)$ (2.23)	Case studies	Slender	Applicable for $\frac{w}{h} \leq 8$

The relations derived from laboratory testing of specimens of various sizes and w/h ratio require excessive extrapolation to estimate the in-situ pillar strengths. Bieniawski (1968) and Mark and Bieniawski (Mark and Chase, 1997) formulae are based on the in-situ testing of coal specimens with the w/h ratio up to 3.4. Hence, they should be used cautiously for estimating the pillar strength for w/h > 3.4.

Sheorey (1993) opined that any formula could be used to estimate pillar strength provided it differentiates failed and stable pillar cases for that condition. He reported that Holland and Gaddy (1957) formula underestimated the pillar strengths for all ranges of w/h. Bieniawski (1992) concluded that the Holland and Gaddy (1957) formula should not be used for greater than 150 m depth as it underestimates the pillar strength in such conditions. The Bieniawski (1968) formula worked well for pillars with w/h<4, it slightly underestimated the strength of the pillar for higher w/h values. While Salamon and Wagner (1985) formula gave an improved estimation of pillar strength for w/h>5 in comparison to the Salamon and Munro (1967) formula, both underestimated the pillar strength in Indian conditions, as they included in-situ strength component having a more significant bias at depth. The database of Salamon and Munro (1967) considered cover depth from 19.8 - 219.5 m, w/h ratio from 0.9 - 3.8 for failed cases and 1.2 - 8.8 for stable cases. Hence, it should not be used beyond these ranges.

Wilson (1972a) formula was derived based on elastoplastic theory for stresses around the circular opening in the failed rock materials, which behaves as Coulomb material. While the method assumed that the stress is uniformly distributed in the core zone, the non-linear distribution of stress in the remaining portion results in the increased overestimation of pillar strength with an increase in the w/h ratio. According to the performance analysis conducted by Sheorey (1993) for failed and stable cases in Indian conditions, the formula underestimated the pillar strength at a lower w/h ratio while it was overestimated for a higher w/h ratio.

Based on the combined database of failed and stable pillar cases from South African and Australian mines, Galvin et al. (1999) developed a linear relation for estimating the pillar strength as the function of the w/h ratio. The combined database had only one case with w/h=8, while the others had w/h<5. Nonetheless, this relation is said to be applicable for all pillars with $w/h \leq 8$.

Mohan et al. (2001) proposed a numerical modelling-based approach for estimating the pillar strength. They considered strain-softening characteristics to model the peak strength of failed and stable cases of coal pillars in Indian conditions. Jaiswal and Shrivastava (2009) employed a Finite Element model to simulate the strength of the coal pillars in India. They considered the post-failure strain-softening behaviour and the variation in dilatancy with the confining stresses and evolution of plastic damage. However, they did not include the effect of confinement at the ends on the pillar strength. The work was limited to simulating the failed and stable cases with $w/h < 5$.

Bertuzzi et al. (2016) noted that the empirical pillar strength formulae are mostly geometry dependent. Therefore, the relative impact of the coal strength, in-situ stresses, and geological discontinuities remain unquantifiable. They employed the extension of damage initiation spalling limit (DISL) approach (Diederichs, 2000; Diederichs, 2007) in conjunction with numerical modelling of failed and stable pillars from a database comprising the collated cases

from Australia, South Africa, USA and India. The approach was able to separate 80 % of the failed and 90% of the stable pillars. The cases which could not be separated by this method had $w/h \leq 4$, denoting very slender or highly rectangular pillars, where the consideration of geological structures becomes inevitable.

2.5 Global Experience of Chain Pillar Design

The chain pillars are an essential structure in the longwall system. One or more rows of chain pillars are provided between panels to ensure the serviceability of gate roads during the life span of the longwall panel. The functional stability of the chain pillar is critical for the safety of the longwall face. In Europe and occasionally in China (Inner Mongolia), rib pillar in the form of continuous coal block (without cross-cuts) is retained between successive longwall panels (Bai et al., 2017). In other parts of the world, including the USA, India, Australia, South Africa, and China, chain pillars are adopted to isolate longwall panels. Chain pillars in the form of yield, abutment, and a combination of abutment and yield pillars have been adopted. In China, a row of yield pillars in conjunction with highly reinforced gate roads is often designed to ensure the serviceability of entries. In contrast, a row of abutment pillars is generally constructed between successive longwall panels to ensure the gate road stability in India, South Africa, and Australia.

In the USA, three entry system consisting of two rows of chain pillars is the most common as this is the minimum number of gate entries required as stipulated by their law to develop the panel entries. However, with increasing panel length, four entries consisting of three rows of chain pillars have become the rule so that the minimum required air quantity can be provided to the face at any distance from the main entries. Sometimes, the gate road system consists of four rows of chain pillars. These chain pillars generally have the configuration of abutment-abutment, yield-abutment, and abutment-yield in case of two rows, and abutment-abutment-

abutment, abutment-yield-yield, abutment-abutment-yield, yield-yield-abutment, abutment-yield-abutment in case of three rows of chain pillars. Although none of these configurations has successfully maintained the gate road stability, the abutment-yield configuration significantly reduces the abutment pressure on the next panel due to a cleaner caving line along the tailgate entry. In the Western US, two and single-entry systems have been employed, but they incur high maintenance costs (Peng and Chiang, 1984).

Chain pillars are designed in US mines based on either a hit-and-trial basis or borrowed from the successful design of other mines (Listak et al., 1988). For example, yield pillars in the various arrangements of the chain pillars are generally of 9-15 m width under the varying depth of cover, geo-mining conditions, and geotechnical properties of the superincumbent strata (Barron et al. 1994). For two rows chain pillars, the size of yield and abutment pillar varies from 12-24m and 24-49m, respectively, for cover depth ranging from 46-762m (Peng and Chiang, 1984).

In Australia, the design of chain pillars is based on the approach which was primarily developed for Bord and Pillar mining method (Seedsman et al., 2005). This approach considers pillar stability as the design criteria. The pillar stability is evaluated using the factor of safety, where Galvin et al. (1999) formula is used to estimate the pillar strength. Colwell (1998) developed an empirical approach called Analysis of Tailgate Serviceability (ALTS) in a similar line to the ALPS method (Mark, 1990; Mark et al., 1994). The design criterion for ALTS is tailgate serviceability. The model has been calibrated considering the loading parameters such as abutment angle and the ratio of the front to side abutment loads for Australian conditions and mining practices.

In India, the design of chain pillars has not garnered much attention. Their dimensions mainly refer to existing regulatory provisions such as Regulation 111 of CMR, 2017 (DGMS, 2017). However, this regulation provides the guideline exclusively for the design of support pillars in

Bord and Pillar workings. The law stipulates that the pillar size should not be less than 48m (c-c) for extraction height of 3m, gallery width of not more than 4.8m, and cover depth exceeding 360m. Another approach for chain pillar design is based on the factor of safety, which includes estimating pillar strength using the Sheorey formula (1987) and pillar load using numerical modelling (Ghosh et al., 2020).

Choi and McCain (1980) proposed a chain pillar design method based on field studies and numerical modelling. They originally developed the technique for a three-entry system with a yield-abutment configuration (an abutment pillar next to a 9.75m yield pillar). In this method, the Tributary Area theory, empirical equations and simplified subsidence model were employed to estimate the development, front abutment and side abutment loads, respectively, while the pillar strength was determined by Holland-Gaddy (1957) formula. The size of the abutment pillar was evaluated using Equation 2.24, as proposed by them. They suggested a safety factor of 1.3 for the optimum design of the pillar.

$$P = 0.6H - 1.2\left[\frac{H^2}{2} - \frac{5}{3}\left(\frac{wl}{l+b} \times \frac{S}{24.9FoS} - wH - \frac{BH}{2}\right)\right]^{0.5} \quad (2.24)$$

where, P is panel width (ft.), H is overburden depth (ft.), w is stiff pillar width (ft.), l is pillar length (ft.), B is entry width (ft.), S is pillar strength, FoS is the safety factor.

Hsuing and Peng (1985) proposed a method for designing a three-entry gate road system with equal-sized pillars based on a three-dimensional Finite Element numerical modelling study. They conducted a parametric study of critical geotechnical parameters such as working depth, pillar width, compressive strength of coal specimens, panel dimensions, modulus of roof and floor, and thickness of the immediate and main roofs and proposed a formula (Equation 2.25) for sizing of chain pillar in three-entry gate road systems. They suggested that the effect of the moduli ratio can be ignored for the preliminary design of the chain pillar.

$$w = -4.676 * 10^{-3}\left(\frac{E_i}{E_c}\right) - 4.04 * 10^{-3}\left(\frac{E_m}{E_c}\right) - 3.33 * 10^{-2} log\left(\frac{E_f}{E_c}\right) - 7.89$$

$$* 10^{-2} log S_c + 0.5144 log H + 4.94 * 10^{-2} log\left(\frac{L}{P}\right) + 0.1941 log P \quad (2.25)$$

where w is chain pillar width (ft.), E_c is the elastic modulus of coal (psi), E_i is the elastic modulus of the immediate roof (psi), E_m is the elastic modulus of the main roof (psi), E_f is the elastic modulus of the floor (psi), S_c is the compressive strength of the coal specimen (psi), H is working depth (ft.), L is longwall panel length (ft.), and P is panel width (ft).

Carr and Wilson (1982) proposed a method to design a chain pillars system for a four-entry longwall system involving a yield-abutment-yield chain pillar configuration. They used the Tributary Area theory and a simplified subsidence model for estimating development and abutment loads, respectively. The Wilson Confined Core model (Wilson, 1982) was used for estimating the pillar strength. Mark and Bieniawski (1986) developed an empirical method called the Analysis of Longwall Pillar Stability (ALPS) method for the design of chain pillars. This method considered the stability of tailgate as the criteria for chain pillar design. The pillar strength was estimated using Bieniawski's (1968) pillar strength formula. The development load of the pillar was determined using the Tributary Area theory, and the abutment loads were evaluated using the following relations:

$$L_s = H^2(tan\beta)\gamma \quad (2.26)$$

$$L_{ss} = \left(\frac{H_p}{2} - \frac{P^2}{8tan\beta}\right)\gamma \quad (2.27)$$

The proportion of abutment load over the chain pillar = $R'L'$

where L'= L_s or L_{ss},

$R' = 1 - \left[\frac{(LTD - w - w_e)}{LTD}\right]^3$ and

$LTD = 5.13\sqrt{H}$ (Peng and Chiang, 1984)

where, L_s and L_{ss} are abutment loads for supercritical/critical and subcritical conditions, respectively (MN/m). H is cover depth (m), P is panel width (m), β is abutment angle (°), and is the unit weight of the rock (MN/m^3), w is chain pillar width (m, solid), and w_e is roadway width (m).

In this method, the chain pillar is designed for the maximum load when the pillar is still part of active longwall mining. Consequently, the maximum load is the summation of the development load, side abutment load due to the first longwall goaf, and the front abutment load due to the second longwall adjacent to the pillar. The front abutment load is estimated as 70% of the side abutment load for the tailgate loading conditions. An abutment angle of 21˚ was suggested for conservative design.

Colwell (1998) developed an empirical method called Analysis of Longwall Tailgate Stability (ALTS) to design chain pillars in Australian coal mining conditions by calibrating the ALPS model based on the field measurement of abutment stress from Australian collieries. He noted that the ratio between the tailgate and main-gate loading conditions of 1.5 and abutment angle of 21° was suitable for characterising abutment load in general Australian conditions. The abutment angle of 26° and the ratio of 1.6 provided a better fit for the Central Colliery. In comparison, the abutment angle of 10° and the ratio of 1.5 was more suitable for Southern Coalfield and the West Wallsend Colliery areas unaffected by sandstone/conglomerate strata close to the coal seam. For other places where the thickening of the sandstone strata occurred, the abutment angle of 10° and the ratio of 3.5 was more appropriate.

According to Wilson (1982), the gate road of the next panel should be located at a distance given by Equation 2.28 from the adjoining extracted panel.

$$w = 2(C + \bar{x}) \tag{2.28}$$

where C is a constant and $\bar{x}$ is the yield zone, which can be determined using Equation (2.29) when roof, seam and floor all have yielded, and Equation (2.30) when only seam has yielded, and roof and floor are rigid.

$$\bar{x} = \frac{h}{2}\left[\left(\frac{\gamma H}{p}\right)^{\frac{1}{(q-1)}} - 1\right] \tag{2.29}$$

$$\bar{x} = \frac{h}{2}\ln\frac{\gamma H}{p} \tag{2.30}$$

where h is the gate road height, H is the cover depth, p is a constant for broken coal (0.1 MPa as suggested by Sheorey (1993); q is the triaxial constant, and γ is the unit weight of overlying rocks. Using the 'stress balance' technique and assuming the exponential decay of vertical stress from its peak to the in-situ value, the constant 'C' can be determined by Equation 2.31 (Figure 2.11).

$$C = \frac{A_w + \gamma H\bar{x} - A_b}{\sigma_0 + (q-1)\gamma H} \tag{2.31}$$

where $A_w = 0.15\gamma H^2$ for critical and supercritical panels ($P \geq 0.6H$), and $A_w = \frac{\gamma P}{2}\left(H - \frac{P}{1.2}\right)$ for subcritical panels ($P < 0.6H$), P is panel width. A_b can be evaluated using Equation 2.32 for yield in the seam, roof and floor, and Equation (2.33) for yield only in the seam and rigid roof and floor.

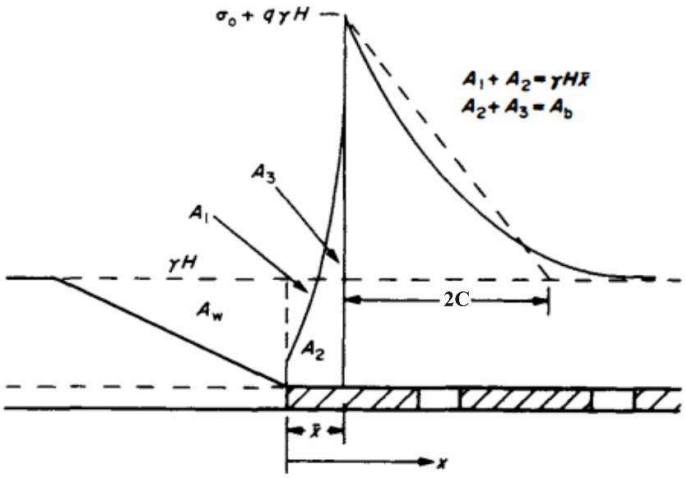

Figure 2.11. Determination of chain pillar width using the load balance scheme (modified after Wilson, 1982)

$$A_b = \frac{hp}{2}\left[\left(\frac{\gamma H}{p}\right)^{\frac{q}{(q-1)}} - 1\right] \tag{2.32}$$

$$A_b = \frac{qh}{F}[\gamma H - p] \tag{2.33}$$

Sheorey (1993) noted that the pillar width determined using this approach varied linearly with the cover depth, which can be hardly accepted. Sheorey et al. (1982a) attempted to evaluate the stability of 18m wide chain pillars surrounded by 4.8m wide gate roads in longwall working with a 150 m wide face at the cover depth of 280m (Figure 2.12). The theory of beams on elastic support was used for estimating side abutment pressure over the pillar with the one-sided goaf and Wilson's (1972a) formula for the long pillar strength estimation. The findings implied that the roadway was distressed even though the chain pillar protecting them was stable.

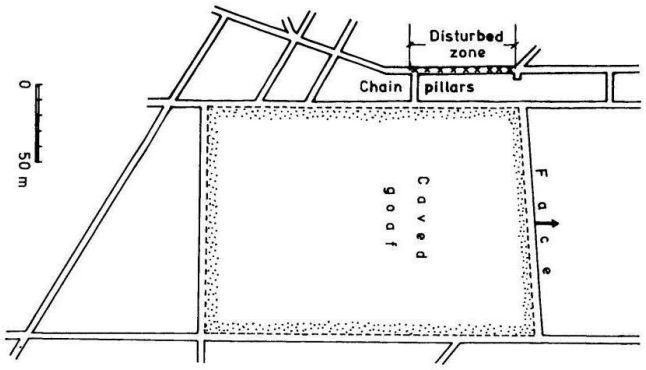

Figure 2.12 Plan showing disturbed zone in the roadway of a longwall panel in Moonidih (after Sheorey et al., 1982a)

Yu et al. (2016) carried out field measurements to assess the change in the vertical stress across a 38 m wide chain pillar with the distance from the retreating longwall face under the weak roof at a depth of 300 – 500 m. They opined that the pillar size could be reduced to 30 m to improve coal recovery, as there were a 10 m wide elastic core in the pillar.

In the past, the numerical modelling technique has been used by several researchers to design and evaluate the chain pillar and gate road stability. Peng and Chiang (1984) used finite difference code to study the stress distribution in the chain pillars in three-entry and four-entry models due to the extraction of longwall panels. They suggested that the average stress in the pillar core should not exceed its triaxial strength to restrict the extension of the yield zone to the other side of the goaf. Shabanimashcool and Li (2012) studied the influence of chain pillar width on the gate road stability and loading to rock bolts of Svea Nord Coal Mine in the Arctic area, where a 250m wide longwall face was extracted beneath the maximum cover depth of 400 m. They found that the maximum load on the rock bolt increased with a decrease in the pillar width, while the bolt failed when the chain pillar width was less than 40m and the cover

depth increased to more than 400 m. The shear displacement along the plane of weakness located 1.5m inside the roof also increased with a decrease in the pillar width, leading to an increased shear loading in a thin pillar than in a wide pillar.

Sinha and Walton (2019a) employed a continuum modelling technique to investigate the mechanism behind the trend of field stress measurement, wherein higher stress was recorded in locations close to the chain pillars compared to those located deeper inside the solid coal. They opined that such observation was primarily because of the reduced flexure of the roof layers and lower compaction of goaf material closer to the pillar. The modelling study by Chokhani (2012) showed that the chain pillar strength increases with the abutment angle. He noted that the factor of safety of the pillar was positively correlated with the pillar width, coal strength, and ratio of moduli of the roof and floor to the coal seam and negatively correlated with the cover depth.

2.6 Important Considerations in the Chain Pillar Design

2.6.1 Safety Factor of Chain Pillar

Determining a suitable factor of safety for the design of chain pillars is challenging. It depends on the approach used for estimating the pillar strength. For example, a pillar strength formula that underestimates the strength would require a lower factor of safety for pillars (Sheorey, 1993). Site-specific empirical strength formula should not be used for other conditions unless it is calibrated against the failed and stable pillar cases. Chain pillars designed for panel isolation have a short life while extracting the second panel. Hence, a low factor of safety is sufficient. Wilson (1972a) recommended a safety factor of 1.0 for such pillars. Sheorey (1993) suggested that a safety factor of 1.0 - 1.5 is adequate for the Sheorey pillar strength formula (Sheorey et al., 1987). Choi and McCain (1980) suggested that a safety factor of 1.3 should be

used to optimise chain pillars. The stability factor in the ALPS and ALTS methods is estimated based on the structural competence of the bolted horizon in the roof. The competence of the bolted horizon is determined based on the Coal Mine Roof Ration (CMRR). The ALPS stability factor (Mark et al. 1994) is given as:

$$\text{ALPS SF}_\text{R} = 1.76 - 0.014\ \text{CMRR} \tag{2.34}$$

The suggested stability factor for the ALPS method is summarised in Table 2.3.

Table 2.3 Suggested stability factor for different competency of roof (Cowell 1998)

	Weak Roof (CMRR=35)	Moderate Roof (CMRR=55)	Strong Roof (CMRR=75)
Suggested ALPS SF	1.3	1.0	0.7
Maximum Entry width (m)	4.3	5.8	6.2

Mark et al. (1998) re-analysed the database of the ALPS method using the Mark-Bieniawski strength equation for rectangular pillars. They obtained a marginally better correlation with 85% of data points correctly predicted by the method. The revised ALPS safety factor is given as:

$$\text{ALPS (R) SF} = 2.0 - 0.016\ \text{CMRR} \tag{2.35}$$

Cowell (1998) suggested the following expressions for evaluating the safety factor of chain pillars for Australian conditions. The Bieniawski formula estimates the pillar strength, with the in-situ coal strength being 6.2 MPa.

$$\text{TG SF}_\text{R} = 2.67 - 0.029\ \text{CMRR} \tag{2.36}$$

2.6.2 Stress-Strain Behaviour of Rocks

The development of stiff servo-controlled testing machines has allowed researchers to study the post-peak behaviour of the rocks. Based on post-peak behaviour, rocks can be categorised into Class I and Class II (Wawersik and Fairhurst, 1970). Class I represents the sudden failure of rock due to uncontrolled propagation and coalescence of the cracks. On the other hand, Class II rock shows the gradual loss of load-bearing capacity due to controlled propagation and coalescence of cracks. The laboratory results of the triaxial loading of rocks at different confining stresses show that the peak and the post-peak strengths (Figure 2.13) and the mode of failure are significantly influenced by the confining stress (Zhao and Cai, 2010; Medhurst and Brown, 1998). The peak and post-peak strengths of the rock increase while the dilatancy decreases with the increase in the confining stresses. Dilatancy defines the increase in the rock volume following the onset of plastic deformation in the rock. The difference between the peak strength and the residual strength also decreases with the increasing confining stresses. Further, a rising trend in the post-failure modulus can also be observed for increased confining stress.

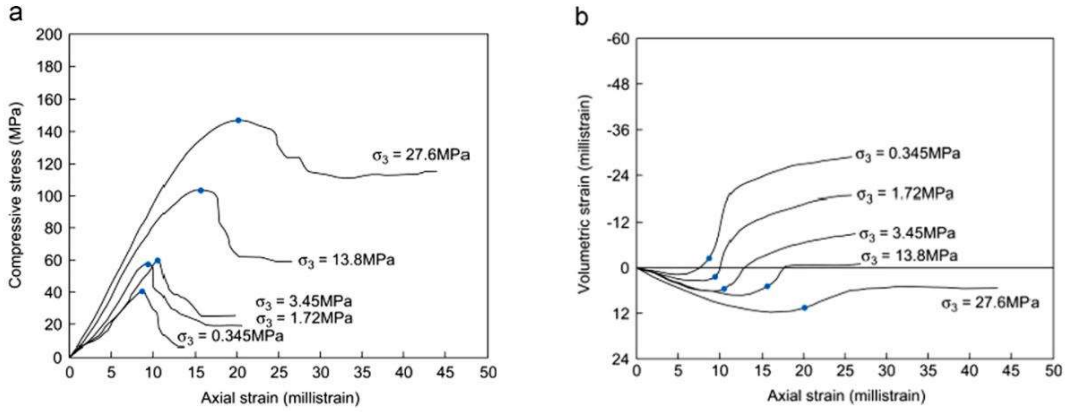

Figure 2.13 Stress-strain curves of the sandstone triaxial tests (Zhao and Cai, 2010)

The laboratory tests conducted by Das (1986) on NX size coal samples of various w/h ratios also confirmed similar trends for strengths and post-peak modulus with variation in the w/h ratio (Figure 2.14). The post-peak behaviour changed from brittle to strain-softening to ductile and then transitioned to strain-hardening with an increasing w/h ratio. The post-failure slope at w/h =13.5 was always positive, implying that such pillars can retain high strength even after failure. The samples having w/h < 4.5 had a highly negative post-failure slope, and they could not retain any post-failure strength because of minimal triaxial confinement at the core. However, the post-failure slope for w/h ≥ 4.5 was positive after its initial negative value because of the reconsolidation of broken coal mass around the core. At w/h of about 10, the post-failure slope becomes zero, showing perfectly ductile behaviour.

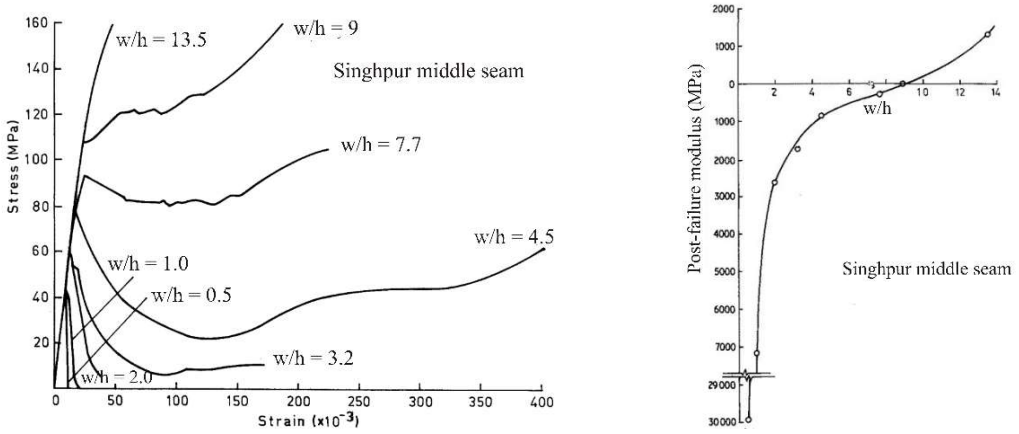

Figure 2.14 Influence of w/h ratio on the post-failure behavior of the coal samples (Das, 1986)

The gradual degradation of the strength with the evolution of plastic damage beyond the peak strength of the rocks has been studied by several researchers (Table 2.4). In the continuum modelling approach, this behaviour of rocks is reproduced by degrading the strength properties

as the function of plastic shear strain. Generally, the residual strength properties are determined based on the back-analysis of failure patterns or deformation within the rock.

It can be noted that while the cohesion of the coal was degraded to its residual value in all studies, the friction angle was either reduced or kept constant or increased. The drop rate and residual value for cohesion varied from 16 - 423 MPa/plastic shear strain and 0 - 35% of the peak value, respectively. The drop rate and residual value of friction angle varied from 400-1200°/plastic shear strain and 71 - 86% of its peak value, respectively. Based on the back-analysis of failed and stable pillars from Indian conditions, Mohan et al. (2001) suggested a constant drop rate and the residual friction angle for different coal strengths. They considered the residual cohesion to be zero in all cases. Although this approach could estimate the peak strength of pillars, it could not model their post-peak behaviour.

Table 2.4 Post-peak strength parameters of the coal used by previous researchers

Reference	Calibration Type	c_{peak} (MPa)	ϕ_i (°)	$c_{res.}$ (MPa)	$\phi_{res.}$(°)	$e_c^{ps}(10^{-3})$	$e_\phi^{ps}(10^{-3})$
Badr (2004)	Peak strength from empirical pillar strength formula	2.1	23	0.105	30	123.6	0.5
Le et al. (2018)	Assumed based on previous studies	1.91	30	0.38	-	5	-
Zhao et al. (2014)	Failure pattern in the sample	1.13	35	0.113	30	50	5
Feng et al. (2019)	Assumed	0.8	24	0.28	21	10	7.5
Zhang et al. (2018)	Peak pillar strength	1.0	30	0.10	24	50	5
Jiang et al. (2017)	Gate road Deformations	1.4	31	0.14	-	1	-
Li et al. (2015)	Peak pillar strength	2.55	34	0.45	-	10	-
Bai et al. (2017)	Stress-strain curve and failure modes from UCS test	4.7	35	0.47	25	10	10
Wang et al. (2015)	Peak pillar strength	2.5	28	0.45	22	10	10
Shabanimashcool and Li (2012)	Bolt load	1.06	29	0.016	-	5	-

Mohan et al. (2001)	Failed and stable pillar cases	c_{peak}	ϕ_i	0	$\phi_i - 5$	10	10
Yan et al. (2013)	Deformations and depth of yield around gate roads	1.2	32	0.03	24	10	10

Dilatancy is a fundamental and pervasive property of the rock (Cook, 1970). In continuum mechanics, dilation angle is widely used to measure dilation. Many researchers have reported that the dilation angle is the function of the confining stress and the inelastic strain in the rock (Detournay, 1986; Alejano and Alonso, 2005; Zhao and Cai, 2010; Walton and Diederichs, 2015; Pourhosseini and Shabanimashcool, 2014). They observed that the maximum dilation rate occurs at the post-failure deformation stage and reaches a constant value beyond the residual strength irrespective of the magnitude of the confining stress. The onset of dilation is delayed, and the increase in dilation decreases with an increase in the confining stress.

Detournay (1986) argued that the dilation must be a function of inelastic strain and confining stress and proposed an exponential function for mobilising dilation. Using the triaxial test results on different sizes of coal samples, Medhurst (1996) reported that the dilation decreased with the increase in the confining stress due to the transition in failure mode from axial splitting to shearing. Alejano and Alonso (2005) re-analysed the tests conducted by Medhurst (1996) and developed a model for the decay of dilation angle with plastic strain. Further, they proposed a formula to estimate the peak dilation angle from the intact compressive strength, friction angle and confining stress. Along similar lines, Zhao and Cai (2010) developed a nine-parameter model for the mobilisation and the decay of the dilation angle with plastic strain. Walton and Diederichs (2015) noted that while Alejano and Alonso (2005) model applies only to sedimentary rocks, a large number of parameters in Zhao and Cai (2010) model makes its implementation cumbersome. They developed an improved model for the dilation angle, which can be used to model the behaviour of brittle rocks. The model considers the phases of the

mobilisation and decay of the dilation as independent segments and requires a relatively small number of parameters.

Several researchers have noted that Young's modulus increases with the increase in confinement (Zisman, 1933; Brown et al., 1989; Cuss et al., 2003; Arzua et al., 2013). A few others considered the average rock modulus under different confining stresses as the representative modulus of the rock (Medhurst and Brown, 1998; Mohan et al., 2001; Jaiswal and Shrivastva, 2009; Pourhosseini and Shabanimashcool, 2014). However, the test results of uniaxial compression tests reported by Das (1986) and Prassetyo (2011) on the coal samples of different w/h ratios did not reveal any contrasting difference in the modulus with the change in the w/h ratio.

2.6.3 Effect of Interface Friction, w/h and w/l Ratios

Numerous studies have shown that the interface friction of coal-roof and coal-floor greatly influences the strength of coal pillars (Iannacchione, 1990; Babcock, 1985; Wagner, 1980; Peng, 1978; Lu et al., 2008; Prassetyo, 2011). Based on the laboratory testing of model pillars of concrete, coal, and rock, Babcock (1985) concluded that the w/h ratio alone is incomplete in pillar design, and the interface effect is a significant variable in pillar strength determination. Babcock (1985) observed that greater confinement is generated in the pillar specimen if the end constraint is provided by steel platens, but tensile stresses are developed along the horizontal plane of the specimen for softer end constraints. The magnitude of the tensile stress also increased with increasing pillar w/h ratio. Consequently, the pillar strength decreases with an increase in the w/h ratio.

Peng (1978) observed that the strength of the cylindrical specimens in the laboratory setup could vary up to 100% depending on the shear strength of the contact surface between the

specimen and the platens. Wagner (1980) demonstrated that a low shear strength contact surface at the top and bottom ends of the specimen influences its strength and changes its mode of failure (Figure 2.15). The laboratory tests conducted by Prassetyo (2011) for various w/h ratios and different types of contact surfaces also showed similar observations.

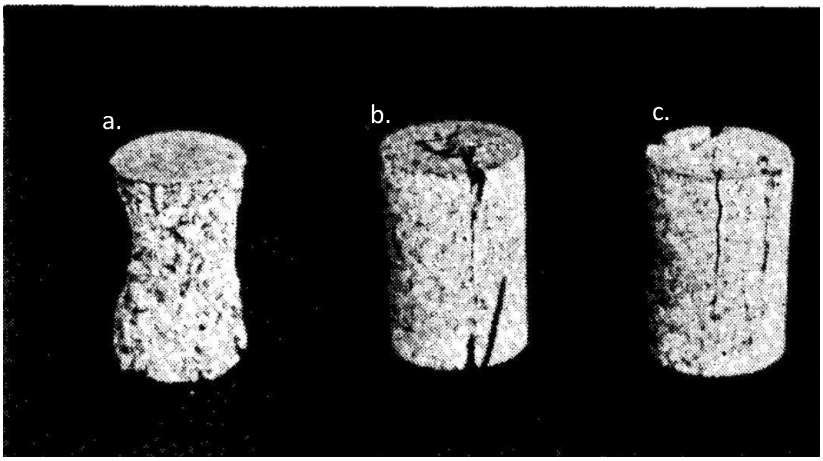

Figure 2.15 Influence of low shear strength contact surface on the mode of failure of the specimen. The specimen on the left, centre and right illustrates the mode of failure when (a) there is no low shear strength contact surface at the lower or upper end, (b) low strength contact surface at both ends, and (c) only on the top contact surface (Wagner, 1978)

Iannacchione (1990) noted that only the strain-softening constitutive model is not sufficient for realistic simulation of the pillar behaviour for a large w/h ratio pillar (w/h>10). Such cases can develop unrealistically high minimum principal stress (confinement) if contact surfaces between the pillar and the surrounding strata are not incorporated into the model. Iannacchione (1990) suggested interface friction of 10 to 20° and cohesion of 0 to 1.03 MPa. Esterhuizen et al. (2010) opined that the interface friction angle should be 25°, and its cohesion should be 0.1MPa for a field representative simulation of stress gradient at the edge of pillars in FLAC^{3D}. They considered normal stiffness of 100 GPa/m and shear stiffness of 50 GPa/m for the interface in the model.

The in-situ tests conducted by Wagner (1974) showed that the pillar failure initiates at the boundary exposed to the free surface and propagates towards the core. The observations showed that the core was subjected to maximum loading after the failure of the pillar and continued carrying load beyond this point (Figure 2.16).

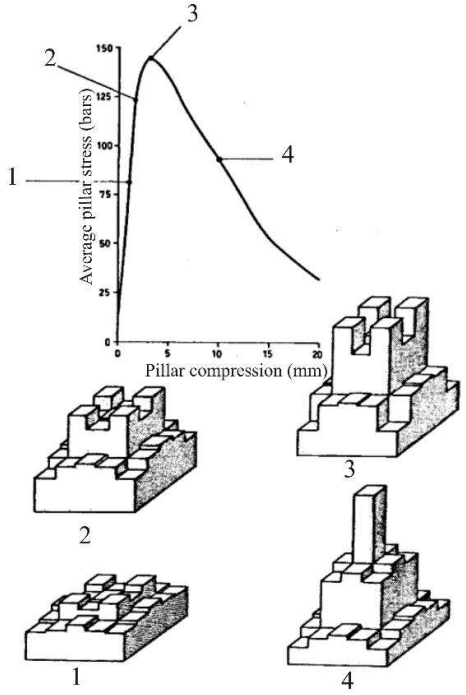

Figure 2.16 Stress-strain characteristics and failure behaviour of an in-situ pillar of 2 m width and 1 m height at different stages of loading (Wagner, 1974)

Morsy (2003) identified three zones in the yield pillar according to their confinement level: Core zone, Transition zone, and Rib zone (Figure 2.17). The core zone is located at the centre portion of the pillar, where plastic deformations are not realised because of relatively high confining stresses. On the other hand, the rib zone covers the ribs and corners of the pillar. As it is exposed to the free space and the low confinement, the pillar yielding begins from this zone and extends towards the core zone. The transition zone, located between the core and the

rib zones, is characterised by a wide range of variations in the confining stress, which increases towards the pillar core.

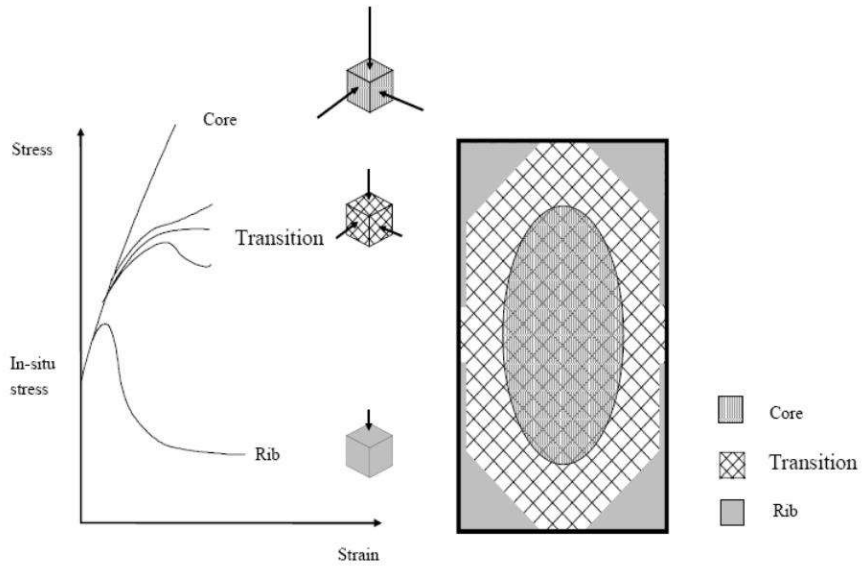

Figure 2.17 The three zones in the yield pillar based on the level of confinement (Morsy, 2003)

The numerical modelling study conducted by Lu et al. (2008) showed that the magnitude of average minimum principal stress and the percentage of the elastic core of the pillar increased with an increase in the w/h ratio and interface shear strength properties (Figure 2.18). The increase of the minimum principal stress with w/h ratio was more pronounced for the increased shear strength of the interface.

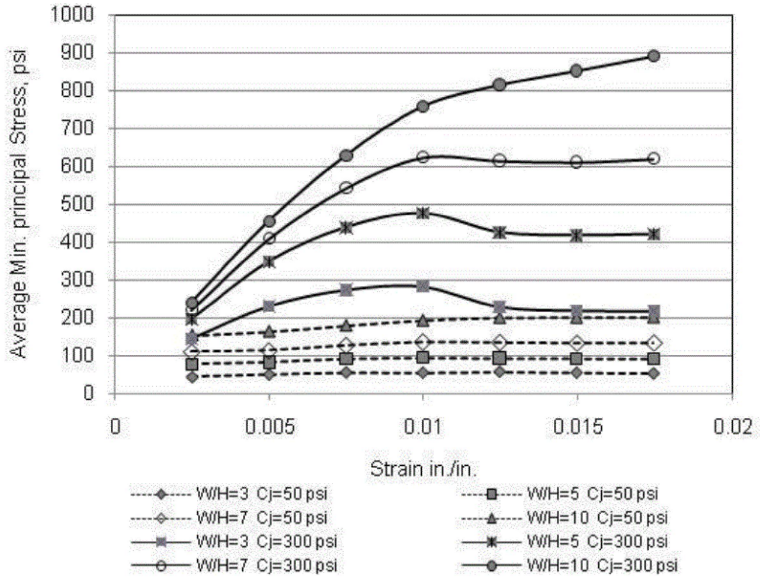

Figure 2.18 The evolution of minimum principal stresses with various w/h ratios and interface properties (Lu et al., 2008)

Similar observations were made by Prassetyo (2011) based on the laboratory testing of coal samples of varying w/h ratios and different interface friction. He identified four distinctive friction zones at the end-surfaces of specimens, indicating the variation of the specimen confinement (Figure 2.19). The core zone occupies the centre of the pillar core with no movement on its surface during the loading history. It does not have any cracks and is highly confined. The intermediate zone is located between the core and the transition zone. The confinement within this zone is less than that in the core zone but greater than the transition zone as the surfaces in this zone have experienced slight friction. Depending upon the w/h ratio, the cracks may or may not initiate in this zone or propagate towards it.

The transition zone occupies the portion between the intermediate and the rib zones. The confinement within this zone is much less than the intermediate zone but greater than the rib

zone, as the surfaces have experienced intense friction. Further, the cracks may have been initiated in this zone or propagated towards it. The rib zone lies between the transition zone and the free surface of the specimen. The confinement in this zone is negligible as it is exposed to the free surface. Hence, this zone yields immediately after the loading, resulting in the initiation and propagation of crack towards the pillar core.

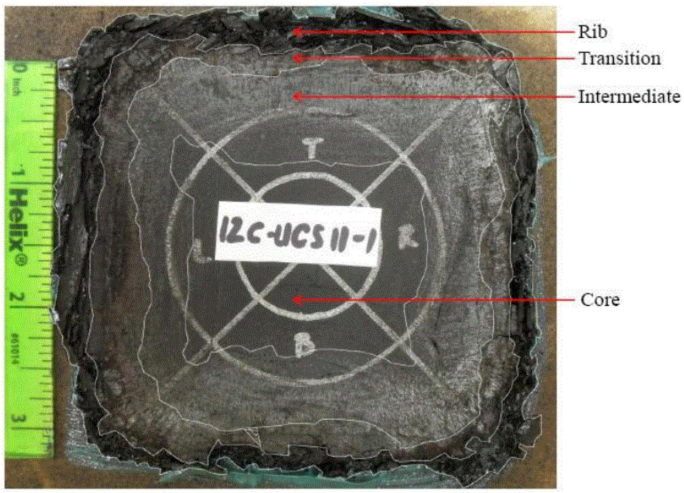

Figure 2.19 The four zones identified on the top end surface of a coal sample of w/h=12 (Prassetyo, 2011)

The empirical formulae of pillar strength are biased towards the square pillars as they are primarily derived from the square pillar database (Section 2.4). Several researchers have introduced the concept of 'effective width' to extend the applicability of these formulae to non-square pillars. Equation 2.37 estimates the effective width (w_{ep}) when the difference between the maximum and the minimum width of the pillar is insignificant.

$$\boldsymbol{w_{ep}} = \sqrt{wl} \tag{2.37}$$

where, w and l are the minimum and the maximum widths of the pillar.

Wagner (1980) suggested Equation 2.38 to calculate the effective width Based on the concept of hydraulic radius.

$$\boldsymbol{w_{ep}} = \boldsymbol{4}\frac{\boldsymbol{A_p}}{\boldsymbol{C_p}} \tag{2.38}$$

where, $\boldsymbol{C_p}$ and $\boldsymbol{A_p}$ are the circumference and cross-section area of the pillar, respectively.

Galvin et al. (1999) found that these methods overestimate the effective pillar width when the maximum width is significantly greater than the minimum width, as the minimum width of the pillar decides the pillar strength in such a case. They opined that the influence of maximum width on the pillar strength could be realized only if the minimum width is more significant than the minimum critical width, which is a function of mining height. Hence, the influence of maximum width on the pillar strength is significantly dependent on its width to height ratio (R). The minimum dimension of the parallelepiped-shaped pillar is given as:

$$\boldsymbol{w} = w \sin \boldsymbol{\theta} \tag{2.39}$$

where w is the minimum width of the pillar and $\boldsymbol{\theta}$ is the acute angle between the adjacent sides of the pillar (Figure 2.20):

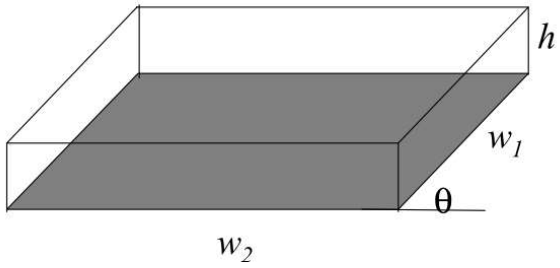

Figure 2.20 The input parameters of the parallelogram-shaped pillar (after Merwe, 2001)

when $\boldsymbol{R_p < R_l}$,

$$\boldsymbol{w_{ep} = w} \tag{2.40}$$

when$\boldsymbol{R_p > R_u}$,

$$\boldsymbol{w_{ep} = w\,\Theta_0} \tag{2.41}$$

$$\boldsymbol{\Theta_0 = \frac{2w_2}{w_1 + w_2}} \tag{2.42}$$

when $\boldsymbol{R_l < R_p < R_u}$

$$\boldsymbol{w_e = w\,\Theta_0^{\frac{R_p - R_l}{R_u - R_l}}} \tag{2.43}$$

where $\boldsymbol{R_l}$ and $\boldsymbol{R_u}$ are limits for the width to height ratio ($\boldsymbol{R_p}$).

In addition, the maximum effective width ($\boldsymbol{w_{ep}}$) ≤ $\boldsymbol{1.5w}$.

Galvin et al. (1999) suggested the reasonable value of $\boldsymbol{R_l}$ and $\boldsymbol{R_u}$ as 3 and 6, respectively. Madden (1988) suggested the critical width to height ratio of 5 for Salamon and Wagner (1985)

squat pillar formula based on w/h range of the failed and stable pillars database for South African conditions.

Dolinar and Esterhuizen (2007) used numerical modelling to study the effect of length on the strength of pillars. They found that length had a substantial influence on the strength of squat pillars but had a negligible impact on the slender pillars. A similar study conducted by Sinha and Walton (2019b) showed that while the strength increased moderately with the length, it is greatly influenced by the w/h ratio compared to the l/w ratio (Figure 2.21). For lower w/h ratios, the strength remained almost constant as the height restricted core formation in the pillar.

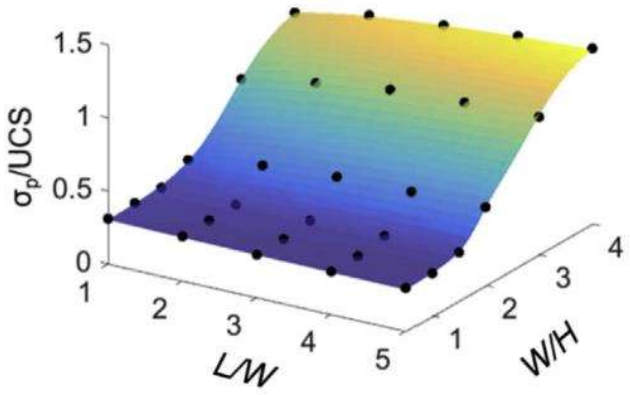

Figure 2.21 Variation of pillar strength with the length to width ratio (l/w) and width to height ratio (w/h). Black dots represent the model predicted pillar strength (after Sinha and Walton, 2019b)

The data compiled from several longwall workings shows that the average length of the chain pillar is 1.5 times the width (Bhaskara, 2022). Under such conditions, the effect of length on the strength of the chain pillar for l/w ratio < 2 is negligible even for pillars of higher w/h ratios.

2.6.4 Constitutive Behavior of the Caved Goaf

In-situ monitoring of stress and deformation in the goaf material is difficult due to the inaccessibility of the goaf area and challenges in maintaining the instruments and lead wires. Several researchers have resorted to indirect methods such as theoretical models, in-situ measurements of stress and deformation in the surrounding structures or laboratory investigations (Pappas and Mark, 1993; Salamon, 1990; Trueman, 1990; Terzaghi, 1965; Sheorey, 1993; Yavuz, 2004; Zhang et al., 2017a) to characterise the constitutive behaviour of the goaf material.

Salamon (1990) proposed a hyperbolic stress-strain relationship (Equation 2.44) to define the constitutive behaviour of the goaf material based on the assumption that it is similar to other granular media like sand and sundry aggregates. In Equation 2.44, σ is the vertical stress, E_0 is the initial tangent modulus, ε is the axial strain and ε_m is the maximum possible compressive strain.

$$\sigma = \frac{E_0 \varepsilon}{\left(1 - \frac{\varepsilon}{\varepsilon_m}\right)} \tag{2.44}$$

Terzaghi(1965) proposed an exponential relationship (Equation 2.45) between stress and strain for the goaf material, where σ is the vertical stress, ϵ is the axial strain, E_o is the initial tangent modulus, and 'a' is a dimensionless constant.

$$\sigma = \frac{E_0}{a}(e^{\epsilon a} - 1) \tag{2.45}$$

Sheorey (1993) developed a set of relations to estimate the elastic modulus of goaf material as a function of distance from the goaf edge and bulk modulus of the goaf as the function of bulk modulus of the host rock. However, Ahmed (2016) opined that these equations could not be used to evaluate the modulus of the caved goaf.

Pappas and Mark (1993) conducted confined uniaxial compression tests on the simulated goaf materials for shale, weak sandstone, and strong sandstone rocks. The simulated goaf material was obtained by shifting the rock size and gradation curve of the actual goaf material to the laboratory scale. They concluded that Salamon (1990) model provides a better representation of the goaf constitutive behaviour across the rock types, whereas Terzaghi (1965) model fails to characterise the behaviour of goaf representing weak rock types (shale and weak sandstone). Yavuz (2004) performed a three-dimensional regression analysis on the test results of Pappas and Mark (1993) to express the initial tangent modulus of the goaf material as a function of bulking factor and intact rock compressive strength. Zhang et al. (2017a) conducted a confined uniaxial compression test on the goaf material following Pappas and Mark (1993) and confirmed that Salamon (1990) model best characterises the behaviour of the goaf material.

2.7 Summary

The review work carried out in this chapter shows that the design of the chain pillar is sensitive to the layout differences between the coal mining countries, the method of estimation of the pillar strength, and the stratigraphy and geo-mining parameters of the overlying strata along with the design criterion. Hence, the approach developed based on the geo-mining conditions of a particular coal mining country cannot be used directly for the conditions of other countries without proper calibration of its parameters (Colwell, 1998). The design of chain pillar is critically dependent on several loading factors such as the cover depth, panel width, abutment angle, the height of damaged zones in the subjacent strata, density and deformation modulus of the overlying strata as well as strength factors such as the pillar width, pillar height, coal strength, and ratio of elastic modulus of the roof and floor strata to that of the coal seam.

The mechanical behaviour of the pillar is critically dependent on the w/h ratio, confining effect provided by the contact surfaces at the pillar ends, post-failure softening and dilatant behaviour,

and the residual strength. The strength of the pillar increases with the increase in the w/h ratio. The brittle post-failure behaviour of the pillar at low w/h ratio transitions gradually to softening at a moderate w/h ratio and then to ductile and hardening at a greater w/h ratio. This behaviour is mostly governed by the confining effect of the contact surfaces and the residual strength of the failed ribs around the core. The pillar with softer end constraints has less strength in comparison to that with stiffer constraints. The dilatancy of the rocks is the function of plastic shear strain and confining stress. The dilatancy gradually decreases with the evolution of plastic damage in the rocks and an increase in confining stress.

The review of pertinent literature regarding the study of the abutment angle indicated that it is not a constant entity. It is the function of the cover depth, panel width, and geo-mechanical properties of the overlying strata. The abutment angle decreases with an increase in the cover depth and panel width. Further, its value is greatly influenced by the geo-mechanical properties of the strata. The abutment angle is higher for strong and competent strata than for soft and weak strata.

The design methods developed in previous works involved estimation of the load using a simplified subsidence model or numerical modelling and the strength using empirical strength formulae. In the simplified subsidence model, the load on the pillar is estimated using the abutment angle concept based on the assumption that the compacted goaf would take the load corresponding to the area bounded by the caving line, defined by the abutment angle, and the caved height. These methods considered a constant abutment angle. The numerical modelling approach has overlooked the strength and deformation properties of the damaged zones in the overlying strata along with the abutment angle in determining the load on the pillar. Further, as these methods involve estimation of strength independently using the empirical formula, they could not assess the confining effect of the abutment angle.

The empirical formulae used for the estimation of the strength of the abutment chain pillar at high cover depth have severe limitations. They were derived based on the database from the failed and stable cases from Bord and Pillar workings with the shallow to moderate cover depth and pillars having w/h < 5 for failed cases and w/h < 8 for stable cases. Further, they did not consider the mechanics involved in determining the pillar strength due to confining effect of the contact surfaces at the pillar ends and the residual strength of the failed pillar ribs.

The review work showed that the design criterion for estimating the optimum size of the chain pillar is highly sensitive to the method of pillar strength estimation. If the method underestimated the strength, a higher value of the safety factor would be required and vice-versa. Hence, this necessitates the evaluation of design criteria specific to the pillar strength estimation method.

The literature review shows that no specific approach exists for designing chain pillars at high depth in the Indian geo-mining conditions, and its design is based on support pillars in Bord and Pillar workings. Further, no attempt has been made to study the pillar stress distribution by employing field measurements in Indian mines. Hence, calibration of the existing approaches for the Indian conditions has severe limitations. A well-calibrated numerical modelling approach is a viable alternative for the chain pillar design as it is a highly cost-effective and efficient tool. Further, the advancement in numerical modelling technique and understanding of the constitutive behaviour of rock has made it possible to realistically model the mechanical behaviour of the goaf material, the rock mass in the Fractured and the Continuous Deformation zones and the complete stress-strain curve of the pillar, for varying w/h ratio along with its dilatancy behaviour.

In light of the above, a well-calibrated numerical modelling approach is required for the design of the chain pillar, considering factors influencing the loading and strength of pillars. The design method should consider redistribution of stresses due to the damaged overlying strata,

sharing of the load by the compacted goaf material, and varying abutment angle with the geo-mining conditions, as they decide the load on the pillar. Further, it should consider the effect of constraints provided by the contact surfaces at the pillar ends and the post-failure softening and dilatancy behaviour for estimating the pillar strength. The design criterion should be devised to ensure the failure of the pillar after the extraction of both the adjoining panels to yield smooth surface subsidence.